Blind modulation format identification using nonlinear power transformation

Research Article | Vol. 25, No. 25 | 11 Dec 2017 | OPTICS EXPRESS 30895
Optics EXPRESS

Blind modulation format identification using nonlinear power transformation

GENGCHEN LIU, ROBERTO PROIETTI, KAIQI ZHANG, HONGBO LU, AND S. J. BEN YOO*

Department of Electrical and Computer Engineering, University of California, Davis, CA 95616, USA
**sbyoo@udavis.edu*

Abstract: This paper proposes and experimentally demonstrates a blind modulation format identification (MFI) method delivering high accuracy (> 99%) even in a low OSNR regime (< 10 dB). By using nonlinear power transformation and peak detection, the proposed MFI can recognize whether the signal modulation format is BPSK, QPSK, 8-PSK or 16-QAM. Experimental results demonstrate that the proposed MFI can achieve a successful identification rate as high as 99% when the incoming signal OSNR is 7 dB. Key parameters, such as FFT length and laser phase noise tolerance of the proposed method, have been characterized.

OCIS codes: (060.1660) Coherent communications; (060.4080) Modulation.

References and links

1. A. Nag, M. Tornatore, and B. Mukherjee, "Optical network design with mixed line rates and multiple modulation formats," J. Lightwave Technol. **28**(4), 466–475 (2010).
2. K. Roberts and C. Laperle, "Flexible transceivers," in *European Conference and Exhibition on Optical Communication* (2012), paper We.3.A.3.
3. M. Xiang, Q. Zhuge, M. Qiu, X. Zhou, M. Tang, D. Liu, S. Fu, and D. V. Plant, "RF-pilot aided modulation format identification for hitless coherent transceiver," Opt. Express **25**(1), 463–471 (2017).
4. S. M. Bilal, G. Bosco, Z. Dong, A. P. Lau, and C. Lu, "Blind modulation format identification for digital coherent receivers," Opt. Express **23**(20), 26769–26778 (2015).
5. F. Khan, K. Zhong, W. Al-Arashi, C. Yu, C. Lu, and A. Lau, "Modulation format identification in coherent receivers using deep machine learning," IEEE Photonics Technol. Lett. **28**(17), 1886–1889 (2016).
6. R. Boada, R. Borkowski, and I. T. Monroy, "Clustering algorithms for Stokes space modulation format recognition," Opt. Express **23**(12), 15521–15531 (2015).
7. X. Mai, J. Liu, X. Wu, Q. Zhang, C. Guo, Y. Yang, and Z. Li, "Stokes space modulation format classification based on non-iterative clustering algorithm for coherent optical receivers," Opt. Express **25**(3), 2038–2050 (2017).
8. T. Bo, J. Tang, and C. Chan, "Modulation format recognition for optical signals using connected component analysis," IEEE Photonics Technol. Lett. **29**(1), 11–14 (2017).
9. P. Isautier, J. Pan, R. DeSalvo, and S. Ralph, "Stokes space-based modulation format recognition for autonomous optical receivers," J. Lightwave Technol. **33**(24), 5157–5163 (2015).
10. I. Fatadin, D. Ives, and S. Savory, "Laser linewidth tolerance for 16-QAM coherent optical system using QPSK partitioning," IEEE Photonics Technol. Lett. **22**(9), 631–633 (2010).
11. L. Huang, D. Wang, A. P. Lau, C. Lu, and S. He, "Performance analysis of blind timing phase estimators for digital coherent receivers," Opt. Express **22**(6), 6749–6763 (2014).
12. F. N. Khan, K. Zhong, X. Zhou, W. H. Al-Arashi, C. Yu, C. Lu, and A. P. T. Lau, "Joint OSNR monitoring and modulation format identification in digital coherent receivers using deep neural networks," Opt. Express **25**(15), 17767–17776 (2017).

1. Introduction

As the global IP traffic continues its exponential growth due to bandwidth-hungry multimedia and cloud services, optical networking is evolving from the conventional fixed "wavelength grid" paradigm toward a flexible and adaptive architecture [1]. By allocating variable bandwidth and modulation formats to each user according to their demand, the next generation flexible and cognitive networks have the potential to significantly increase the total traffic [1]. With a view toward an intelligent network, flexible transceivers that can

#303850 https://doi.org/10.1364/OE.25.030895
Journal © 2017 Received 1 Aug 2017; revised 25 Oct 2017; accepted 19 Nov 2017; published 27 Nov 2017

Optics EXPRESS

support the transmission and reception of variable modulation formats have gained a significant amount of research interest [2,3]. One important building block of a flexible receiver is the modulation format identification (MFI) module, which tracks the modulation format of the received signal and reconfigures the digital signal processing (DSP) circuit of the receiver accordingly. As discussed in [3–9], this automatic recognition functionality removes the need for end-to-end handshaking between the transmitter (Tx) and receiver (Rx).

Various MFI techniques have been proposed recently [3–9]. For example, Bilal *et al.* introduced a blind MFI by evaluation the *peak-to-average power ratio* (*PAPR*) of the incoming samples after chromatic dispersion (CD) compensation and constant modulus algorithm (CMA) equalization [4]. However, the *PAPR* for different modulation formats is highly dependent on the optical-signal-to-noise ratio (OSNR) of the incoming signal. Therefore, an additional OSNR monitor is required before the MFI module. In [5,12], accurate MFI as well as OSNR monitoring can be achieved by using a deep neural network (DNN). Yet, extensive training data sets for the DNN are required. MFI can also be realized in Stokes space [6–9] by using K-means clustering, connected component analysis (CCA) or image processing techniques.

In order to maintain a satisfactory identification accuracy (>99%), most of the *blind* MFI techniques in the literature require high OSNR values. For instance, in [4–9], to achieve over 90% of correct classification rate, the incoming 16-QAM signal requires at least 19 dB OSNR. This is because the ASE noise at low OSNR values significantly affects the signal power distribution and hence deteriorates the classification accuracy.

In this paper, a noise-tolerant MFI scheme based on nonlinear power transformations and peak detection is proposed. By applying specific power operations to the incoming signal, the proposed scheme generates a spectral peak tone whose amplitude depends on the modulation format. Experimental results demonstrate that the proposed method has high noise-tolerance, achieving over 99% of successful identification rate when the incoming signal has an OSNR as low as 7dB, for BPSK, QPSK, 8-PSK, and 16-QAM.

2. Principle of operation

Figure 1 shows the architecture of a flexible receiver that supports automatic reception of signals with different modulation format. Chromatic dispersion (CD) compensation and clock recovery are performed at the beginning of the DSP chain as they are transparent to different modulation formats. When the system employs dual-polarization transmission, constant-modulus algorithm (CMA) based equalizer is also required for polarization demultiplexing before the MFI stage. The MFI estimates the modulation format of the incoming signals and reconfigures the modulation format dependent DSPs, such as the adaptive equalizer, frequency offset estimator (FOE), and carrier phase recovery (CPR).

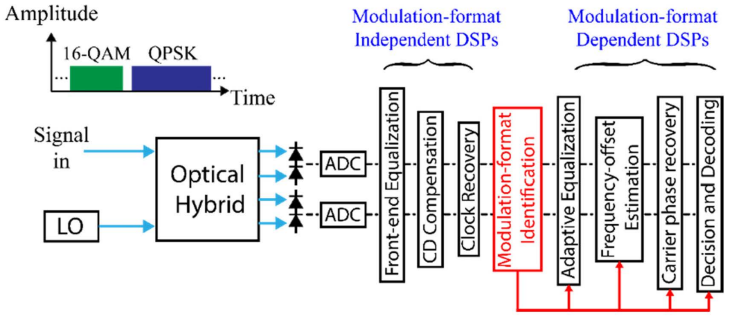

Fig. 1. Flexible receiver DSP architecture with blind MFI stage. LO: local oscillator; ADC: analog to digital converter. Inset in the top left shows incoming signals with different modulation formats.

Optics EXPRESS

After CD compensation and clock recovery, the k^{th} received sample by the MFI block with one sample per symbol duration can be expressed as:

$$X_k = A_k \cdot e^{j(\omega_c k T_s + \varphi_k)} + n_k \tag{1}$$

where A_k is the complex modulated data, ω_c is the frequency offset, T_s is the symbol duration, φ_k is the phase noise induced by the carrier and LO laser's linewidth, and n_k is the complex additive white Gaussian noise (AWGN). For a block of N samples X_k, X_{k+1}, ……, X_{k+N-1}, it can be considered as a *discrete-time random process* $\boldsymbol{X}$, and its Fourier transform can be decomposed as,

$$F\{\boldsymbol{X}\} = F\{\boldsymbol{S}\} + F\{\boldsymbol{N}\} \tag{2}$$

where $\boldsymbol{S}$ is composed of $A_k \times \exp(j\omega_c k T_s + \varphi_k)$, ……, $A_{k+N-1} \times \exp(j\omega_c (k+N-1) T_s + \varphi_{k+N-1})$, and $\boldsymbol{N}$ denotes the discrete-time AWGN process. Since the modulated data are independent of the laser phase noise, $\boldsymbol{S}$ can be further expanded as $\boldsymbol{S} = \boldsymbol{A}\boldsymbol{\Phi}$, where $\boldsymbol{A}$ includes the complex modulated data sequence and $\boldsymbol{\Phi}$ comprised of the intermediate frequency (IF) and phase noise terms. Since each element of $\boldsymbol{A}$ (the modulated data) are *independent and identically distributed* (i.i.d) random variables, the spectral property of $\boldsymbol{A}$ can be evaluated by calculating its statistic autocorrelation:

$$R_A[k, k+m] = E[A_k \cdot A_{k+m}^*] = E[A_k] \cdot E[A_{k+m}^*], \quad m \in [0,1,\ldots N-1] \tag{3}$$

For BPSK signal, A_k is randomly chosen from {-1, 1} with equal probability, thus the statistic autocorrelation of $\boldsymbol{A}$ becomes:

$$R_A[k, k+m] = \begin{cases} 0, & m \neq 0 \\ 1, & m = 0 \end{cases} \tag{4}$$

Therefore, the power spectral density (PSD) of $\boldsymbol{A}$ can be calculated by computing the length-N fast Fourier transform (FFT) of the autocorrelation. Since the autocorrelation of $\boldsymbol{A}$ is a time-domain impulse, its energy is uniformly distributed along the entire frequency range. Because the FFT of $\boldsymbol{\Phi}$ is simply a phase noise corrupted pulse function with Lorentzian shape centered at ω_c or folded frequency of ω_c, and $\boldsymbol{N}$ is a white Gaussian process, the energy of $\boldsymbol{S}$ and $\boldsymbol{X}$ is also uniformly distributed over the spectrum. This property applies to all modulation formats with the symmetric constellation, such as BPSK, QPSK, 8-PSK, and 16-QAM. On the other hand, if we raise X_k to the power of two, shown as:

$$(X_k)^2 = A_k^2 \cdot e^{2j(\omega_c k T_s + \varphi_k)} + n_k^2 + 2A_k n_k e^{j(\omega_c k T_s + \varphi_k)} \tag{5}$$

Now $\boldsymbol{X}$ becomes $(X_k)^2$, $(X_{k+1})^2$, ……, $(X_{k+N-1})^2$, its Fourier transform can be decomposed as:

$$F\{\boldsymbol{X}\} = F\{\boldsymbol{S}\} + F\{\boldsymbol{N}\} + F\{\boldsymbol{N}'\} \tag{6}$$

where $\boldsymbol{N}'$ denotes the product of original samples and AWGN. Using the same expanding procedures shown above ($\boldsymbol{S} = \boldsymbol{A}\boldsymbol{\Phi}$), we can write down the statistic autocorrelation of $\boldsymbol{A}$. Noticed that now process $\boldsymbol{A}$ consists of $(A_k)^2$, $(A_{k+1})^2$, ……, $(A_{k+N-1})^2$. For BPSK signal, $(A_k)^2$ becomes constant for all k, therefore its autocorrelation is also a constant and a strong peak tone shows up in its PSD:

$$R_A[k, k+m] = 1, \quad m \in [0,1,\ldots N-1] \tag{7}$$

$$S_A(f) = \delta(f) \tag{8}$$

The peak tone will be preserved after the convolution with the frequency offset/phase noise term $\boldsymbol{\Phi}$, and the addition of the noise term $\boldsymbol{N}$ and $\boldsymbol{N}'$, since both $\boldsymbol{N}$ and $\boldsymbol{N}'$ are also uniform across all the frequencies. For other modulation formats, such as QPSK signal, $(A_k)^2$

Optics EXPRESS

becomes a BPSK-like data sequence, and no peak tone will show up in the frequency domain. To generate a peak tone, A_k needs to be raised to the power of four for QPSK and 16-QAM, and power of eight for 8-PSK.

In conclusion, we can identify the unknown modulation format by evaluating the peak to average ratio of the Fourier transform of the received samples after different power operations. Because the correct power operation squeezed all the energy into one spectral location where the peak tone is located, the proposed method gains excellent noise tolerance compared with the other MFI methods in the literature discussed in the introduction. Figure 2 illustrates different modulation formats and their 512-point FFT after the nonlinear power transformations. The signals in Fig. 2 are obtained from simulations, with 10 GBd baudrate, 100 kHz laser linewidth, and 500 MHz frequency offset. With 6 dB OSNR, it is challenging to distinguish between the BPSK, QPSK, and 8-PSK from their amplitude histograms directly. However, after performing the correct power operation, a peak tone will show up on the frequency spectrum of the signal. By evaluating whether there is a peak tone or not after certain transformations, it is possible to determine the modulation format of the signal.

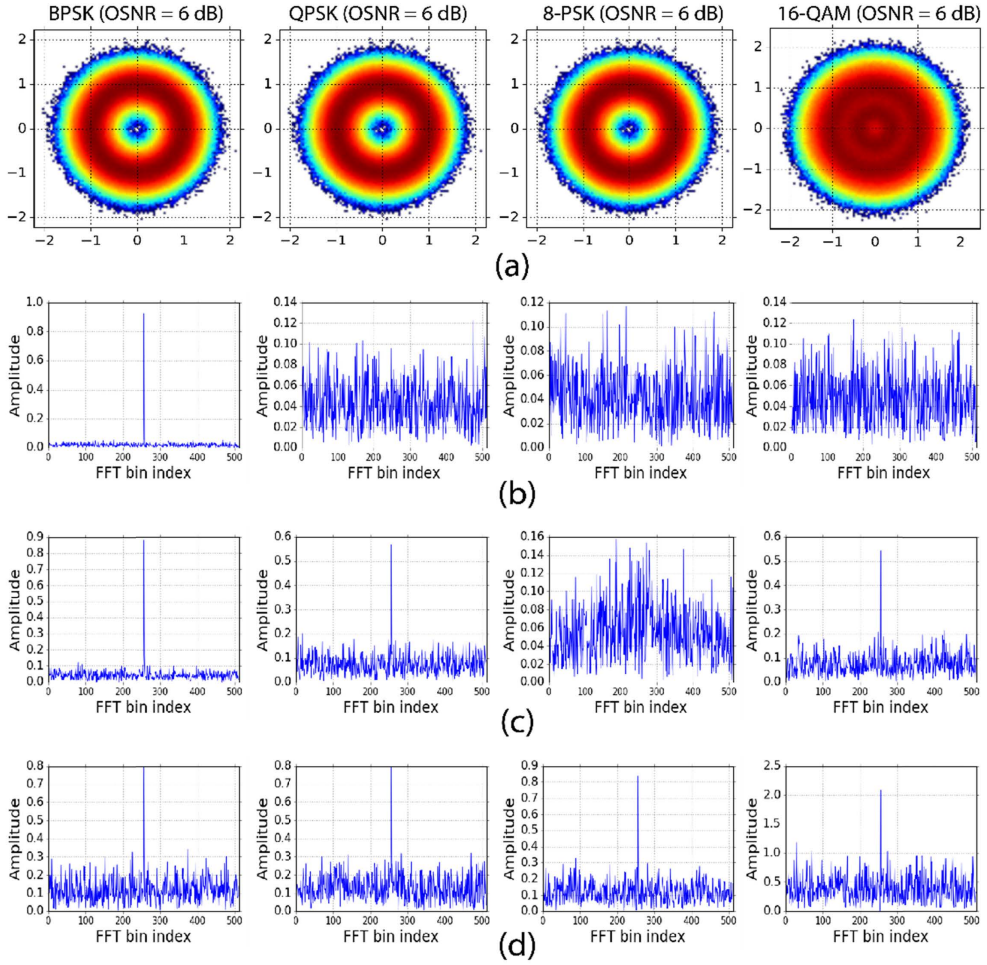

Fig. 2. (a) Constellation diagrams. (b) FFT after $()^2$. (c) FFT after $()^4$. (d) FFT after $()^8$.

From Fig. 2, it could be noted that QPSK and 16-QAM signals have similar properties. They both generate a peak tone after the power of four or power of eight operations, so they

Optics EXPRESS

cannot be distinguished directly. Inspired by the radius-directed approach proposed by Fatadin *et al* [10], QPSK partition can be performed as shown in Fig. 3. The proposed MFI realizes the partitioning by discarding all the samples whose amplitude varies between 0.724 and 1.171. By doing so, the MFI conserves the outermost and innermost 4 symbols of the 16-QAM while discarding most of the symbols for the QPSK signal. After the partition and fourth power operation, 16-QAM signal will show a clear line on its amplitude spectrum whereas QPSK will not. A complete list of the generated peaks in the spectrum after different nonlinear power transformations to the signal can be found in Table 1. Peak detection can be performed by calculating the peak to average power ratio (*PARR*) of the received signal after the transformation and FFT:

$$PAPR = \frac{\max(|F\{\boldsymbol{X}^{2\ or\ 4\ or\ 8}\}|)}{\mathrm{mean}(|F\{\boldsymbol{X}^{2\ or\ 4\ or\ 8}\}|)} \tag{9}$$

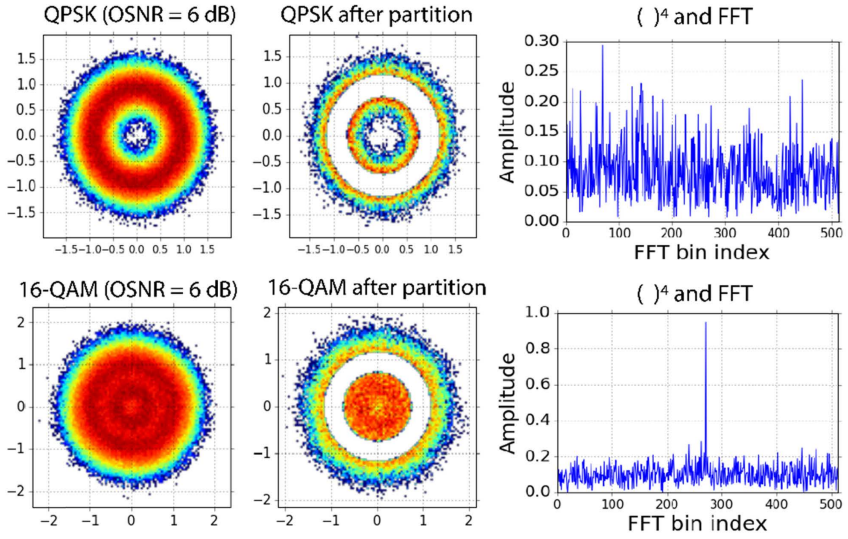

Fig. 3. Distinguish between QPSK and 16-QAM.

Table 1. Peak generated by different nonlinear transformations

Transformations	BPSK	QPSK	8-PSK	16-QAM
$()^2$	Peak	No peak	No peak	No peak
$()^4$	Peak	Peak	No peak	Peak
$()^8$	Peak	Peak	Peak	Peak
Partition & $()^4$	No peak	No peak	No peak	Peak

The *PAPR* threshold should be chosen to minimize the probability of missed alarm (neglect a peak tone) and false alarm (mistakenly recognize a deceptive peak tone) of the proposed MFI. We conducted numerical simulations with 10 GBd BPSK, QPSK, 8-PSK, and 16-QAM signal at 10 dB OSNR to investigate the effect of different *PAPR* values. 20 independent simulations for each modulation format with 2^{20} samples are tested. The FFT size for each MFI is 2^{10} and the laser linewidth for all simulations is set to 100 kHz. We swept the PAPR threshold from 0 to 35 and calculated the probabilities of missed alarm and false alarm. Figure 4 shows the probabilities of missed alarm and false alarm for different PAPR thresholds. When the *PAPR* threshold is low, the proposed MFI would produce frequent false alarms, leading to a modulation format recognition failure. As the *PAPR* threshold increases, the false alarm rate of the proposed MFI is reduced. If we increase the *PAPR* threshold

Optics EXPRESS

further, the system starts missing the peak tone due to the reduction of peak detection sensitivity. For BPSK signal, we didn't observe any missed alarm during the simulation. In this study, we used 5 as our *PAPR* threshold.

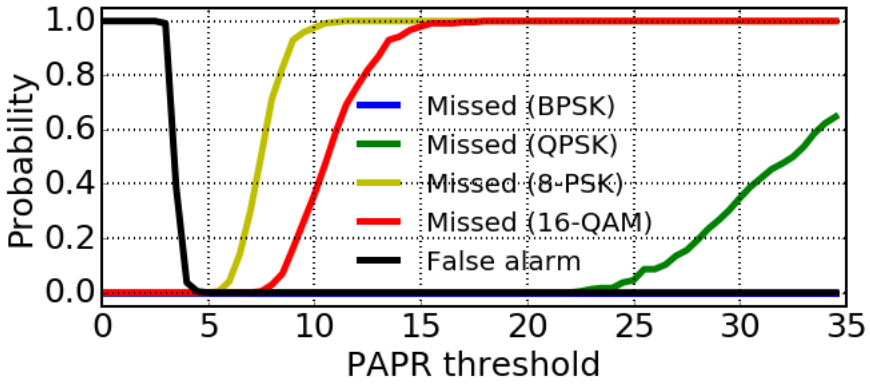

Fig. 4. Probabilities of missed and false alarm versus the *PAPR* threshold.

3. Experimental results

To characterize the performance of the proposed MFI, we conducted a 10 GBd transmission experiment. The experimental setup used in this study is shown in Fig. 5(a). A 30-kHz linewidth external cavity laser (ECL) operating at 1551.75 nm is used as the Tx laser. The Tx laser is modulated as 10 GBd BPSK, QPSK, 8-PSK, and 16-QAM using a LiNbO3 modulator and a Tektronix electrical arbitrary waveform generator (EAWG) at 12 GS/s. The output of the I/Q modulator is fed to a noise loader or a 300-km fiber span, which consists of 150-km standard single mode fiber (SSMF) and 150-km dispersion shifted large-effective-area fiber (LEAF). After the transmission, the optical signal is coherently detected by a coherent receiver with a local oscillator (LO). The linewidth of the LO is 100-kHz. We use a Tektronix real-time scope to sample the detected signal at 50 GS/s and apply offline DSP, shown in Fig. 5(b), to the signal. First, the RX performs front-end equalization, such as skew and I/Q gain adjustment to the received waveform. Next, the signals are match-filtered and resampled to 20 GS/s. After clock recovery with Godard's method [11], the signals are launched into the proposed MFI block for modulation format recognition. The modulation format information extracted from the received signal is then used to select the proper subsequent DSP blocks. We utilize the classic time-domain, M^{th} power based frequency offset estimator with 2^{12} block-length and the blind phase search (BPS) method with 20 test angles and 9 average lengths for carrier recoveries.

Optics EXPRESS

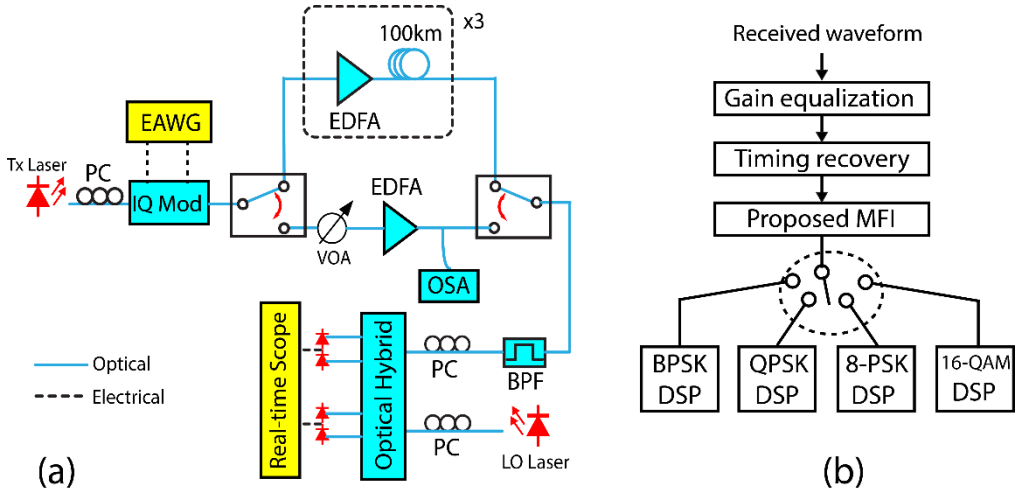

Fig. 5. (a) Experimental setup. VOA: variable optical attenuator. BPF: bandpass filter. OSA: optical spectrum analyzer. PC: polarization controller. EDFA: erbium-doped fiber amplifier. (b) DSP flow of the receiver.

Figure 6(a) shows the implementation architecture of the proposed MFI. The complex samples are split into four copies, which undergo different nonlinear operations as shown in Table 1. After that, MFI scheme applies FFT to the transformed samples and do the peak detection by calculating the *PAPR* and comparing with the threshold for each path. If the calculated *PAPR* is larger than the threshold, the output of the peak detection unit d_i will be asserted. Otherwise, d_i remains zero. The peak information is then passed through a lookup table (LUT)-based decision tree shown in Fig. 6(b). The output of the LUT indicates the modulation format of the input signal.

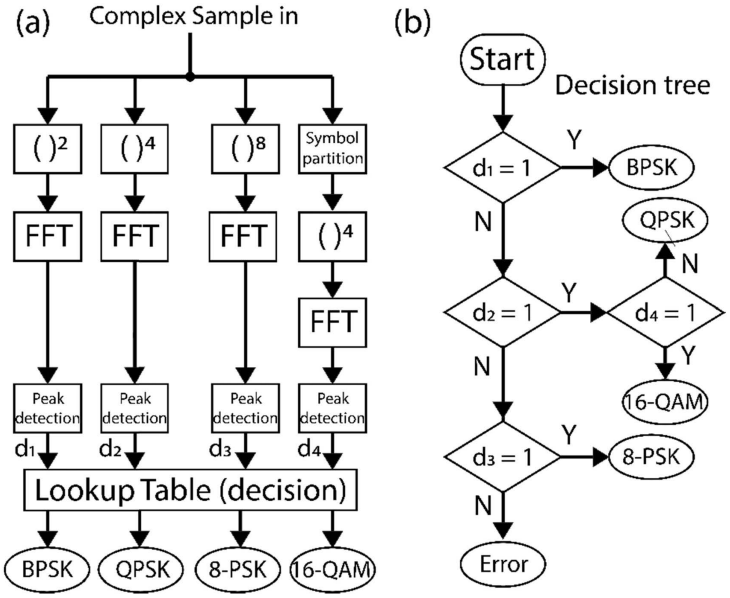

Fig. 6. (a) Proposed MFI block diagram. (b) Flow chart of the decision tree.

The experimental results are plotted in Fig. 7 with different FFT length. The total number of symbols was 400,000 for each modulation formats. It is evident from the figure that the correct recognition rate for all modulation formats exceeds 99% at 7 dB OSNR when the FFT

Optics EXPRESS

length is larger than 2^{10}, which indicates the strong noise-tolerance of the proposed MFI. Comparing with other modulation formats, 8-PSK requires slightly higher OSNR to achieve the same correct recognition rate. This is due to the fact that, unlike the 2nd power operation in (5), the 8th power operation introduces more noise terms, such as S^7N, S^6N^2 and so on. As we increase the FFT length, more energies are squeezed into the peak tone after the correct power transformation, which results in higher successful recognition rates for all modulation formats.

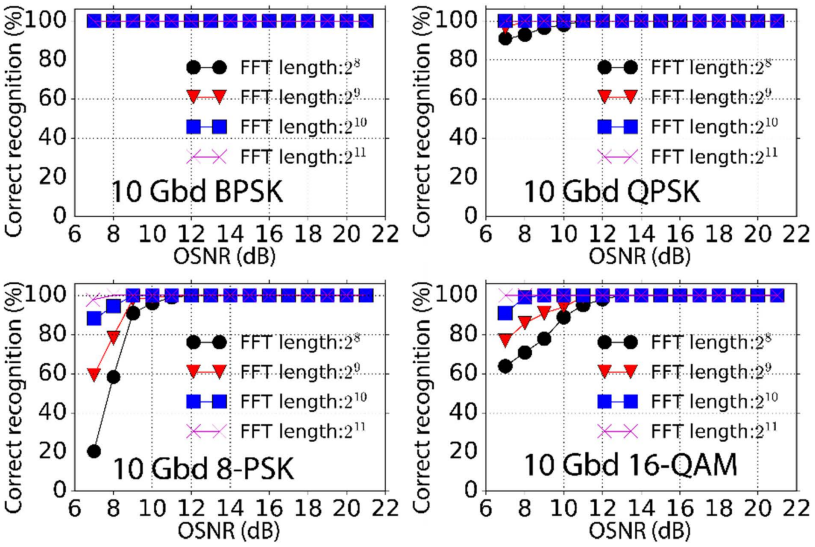

Fig. 7. Measured probability of correct recognition for 10 Gbaud BPSK, QPSK, 8-PSK, and 16-QAM signals with variant length of FFT.

To investigate the effect of laser phase noise on the proposed MFI, we replace the 100-kHz linewidth LO with a 2-MHz linewidth laser. Figure 8 shows the 2^{10} points FFT results for 16-QAM signal after 4th power operation using different LO lasers at 10 dB OSNR. Clearly, the presence of larger phase noise corrupts the generated peak tone, resulting in the reduction of the *PAPR*. Figure 9 depicts the power penalty of the proposed MFI with 2-MHz linewidth laser against 100-kHz linewidth laser. The FFT length is set to 2^8. Approximately 3 dB OSNR penalty was observed for QPSK, 8-PSK, and 16-QAM signals at the correct recognition rate of 85%, 65%, and 62%, respectively. This power penalty is universal regardless of the FFT size. Because increasing the length of FFT cannot reduce the energy leakage of the peak tone induced by the laser phase noise.

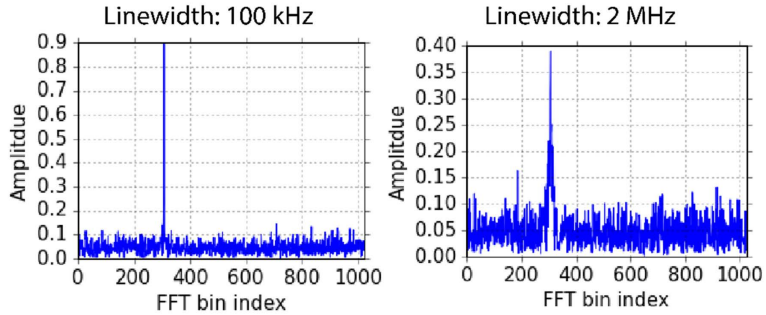

Fig. 8. Energy leakage induced from the larger phase noise for 16-QAM signal after 4th power operation.

Optics EXPRESS

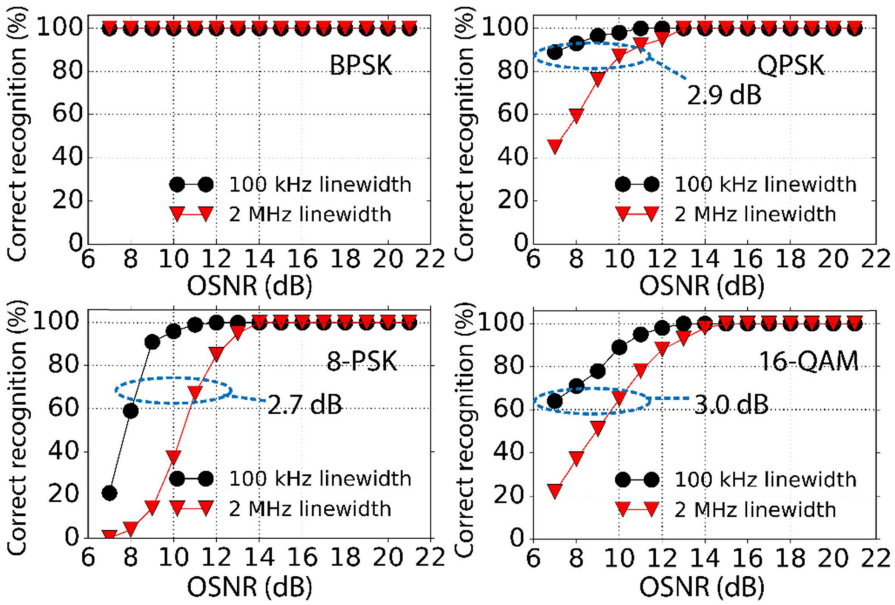

Fig. 9. Measured probability of correct recognition for different modulation formats with 100 kHz and 2 MHz linewidth lasers.

To evaluate the effect of fiber nonlinearity on the proposed MFI, we conduct 300-km (150-km SMR and 150-km dispersion shifted fiber) transmission experiment for QPSK and 16-QAM signals by adjusting the launch power of the fiber span. The results of the transmission experiment are shown in Fig. 10, with 2^{10} FFT lengths. For up to 3 dBm launch power, 100% correct identification can be realized for QPSK and 16-QAM signals. The insets in Fig. 10(a) show the demodulated constellations of 16-QAM signal with 3 dBm and –9 dBm launch power. Clearly, with 3 dBm launch power, the 16-QAM signal undergoes a "vortex-like" distortions due to the fiber nonlinearities. Since the symmetric property of the constellation is not significantly affected by the "vortex-like" distortion, the spectral peak tone after nonlinear power transformation can still be preserved. Figure 10(b) depicts the measured *Q*-factor of the transmission experiment.

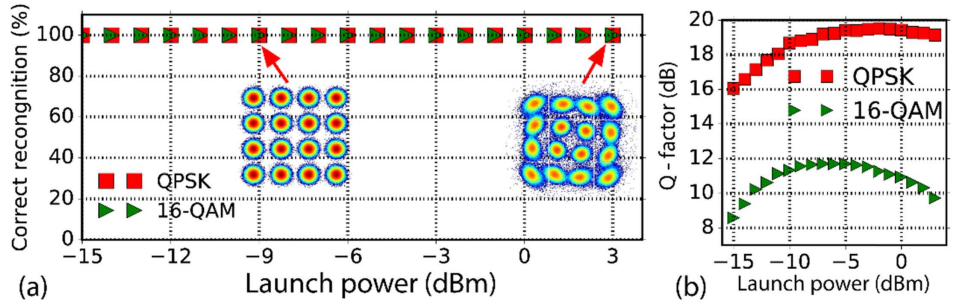

Fig. 10. (a) Measured probability of correct recognition for different launch power. (b) Measured *Q*-factor for different launch power.

In Fig. 11, the minimum OSNR required for each MFI to achieve over 99% of estimation accuracy is shown [4–9]. Each data point of the minimum OSNR is obtained based on the best value (minimum OSNR value to achieve over 99% accuracy) reported in the literature except for the proposed MFI. Missing bars are denoted by asterisk symbols and represent the cases where the corresponding method has not been applied to that modulation format.

Optics EXPRESS

Superior OSNR performance could be achieved by using the proposed MFI compared with other methods in the literature. In particular for 16-QAM signal, the proposed method reduces the minimum required OSNR by approximately 11 dB against other MFIs.

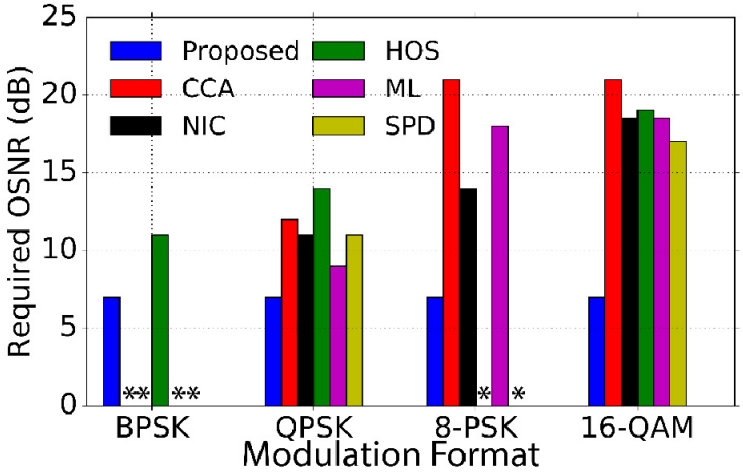

Fig. 11. Minimum OSNR required for identification of modulation formats for different MFIs CCA: Connected component analysis [8], 32 GBd. NIC: Non-iterative clustering [7], 28 GBd 80-km SMF. HOS: Higher-order statistics [9], 31.5 GBd, 810-km LAF. ML: Maximum likelihood [6], 28 GBd B2B. SPD: Signal power distribution [4], 14 GBd B2B.

In our proposed MFI, the most computation intensive process is the FFT block. As the required multipliers for each FFT block grows as $N\log(N)$, the total hardware complexity of the MFI in this work is higher than the time-domain methods [4]. However, it should be noted that the proposed MFI can also be used for frequency offset (FO) estimation, as it composed of all the necessary circuit components of the classic Viterbi-Viterbi frequency-domain frequency offset estimator (FOE). By recording the location of the generated peak tone, the FO between the carrier signal and LO can be calculated. Therefore, considering the fact that the standalone FOE can be taken away when utilizing the proposed MFI, the equivalent hardware complexity of the receiver is not strongly affected.

Although we only covered BPSK, QPSK, 8-PSK, and 16-QAM in this study, it should be noted that the proposed MFI can also be applied to higher-order modulation formats such as 32-QAM and 64-QAM. Both 32-QAM and 64-QAM signals can generate a peak tone after 4th power operation and FFT because of the QPSK-like symbols located on the diagonal lines of the complex plane. By applying proper partitioning technique (for example, filtering out the 32-QAM symbols while keeping the QPSK-like symbols for 64-QAM), we could achieve MFI for 32-QAM and 64-QAM signals as well. However, as the order of modulation formats increases, the limited Euclidean distance between the individual symbols of M-QAM signals poses substantial difficulties on efficient symbol partitioning, resulting in the reduction of the *PAPR*. For this reason, the proposed MFI should utilize longer FFT for higher-order QAM signals to compensate the imperfect partition.

4. Conclusion

In this paper, we report a noise-tolerant MFI method based on nonlinear power transformation. To the best of our knowledge, the proposed method offers strongest noise tolerance against all the other *blind* MFIs in the literature. Experimental results demonstrate that the proposed MFI can maintain high identification accuracies (> 99%) for BPSK, QPSK, 8-PSK, and 16-QAM even at low OSNR (~7 dB).